Multifractal properties of the harmonic measure on Koch boundaries in two and three dimensions

D. S. Grebenkov,[1,*] A. A. Lebedev,[1] M. Filoche,[1,2] and B. Sapoval[1,2]
[1]*Laboratoire de Physique de la Matière Condensée, C.N.R.S. Ecole Polytechnique, 91128 Palaiseau, France*
[2]*Centre de Mathématiques et de leurs Applications, C.N.R.S. Ecole Normale Supérieure, 94140 Cachan, France*
(Received 9 December 2004; published 27 May 2005)

The multifractal properties of the harmonic measure on quadratic and cubic Koch boundaries are studied with the help of a new fast random walk algorithm adapted to these fractal geometries. The conjectural logarithmic development of local multifractal exponents is guessed for regular fractals and checked by extensive numerical simulations. This development allows one to compute the multifractal exponents of the harmonic measure with high accuracy, even with the first generations of the fractal. In particular, the information dimension in the case of the concave cubic Koch surface embedded in three dimensions is found to be slightly higher than its value $D_1=2$ for a smooth boundary.

DOI: 10.1103/PhysRevE.71.056121 PACS number(s): 02.50.Cw, 05.10.Ln, 05.45.Df, 05.60.−k

I. INTRODUCTION

The scaling properties of the harmonic measure on fractal curves have been studied intensively [1,2]. This measure provides an efficient mathematical tool to describe the accessibility of a boundary for Brownian motion. For these reasons, it is involved in various phenomena: random growth processes (e.g., diffusion-limited aggregation), primary current distribution in electrochemistry, distribution of particle flows on a membrane, and electric charge distribution on a metallic surface. By studying the harmonic measure on a fractal curve, one can determine how it varies on different scales with the help of so-called multifractal exponents $\tau(q)$. In the two-dimensional case, there are important theoretical and numerical results. In particular, the famous Makarov's theorem [3] states that the information dimension of the harmonic measure on a simply connected two-dimensional set is equal to 1. This mathematical result has important consequences in physics [4,5].

The three-dimensional case is drastically more difficult for theoretical and numerical reasons. At the same time, it is the most important case for practical applications.

The present paper is devoted to the numerical study of the harmonic measure on quadratic and cubic concave Koch boundaries with Hausdorff dimensions $D_0=\ln 5/\ln 3$ and $D_0=\ln 13/\ln 3$, respectively, shown in Fig. 1. The main goal of this paper is the accurate determination of the multifractal exponents in a numerical way. For these purposes, we first guess a logarithmic development of the local multifractal exponents allowing one to compute the multifractal exponents accurately (Sec. II). Then, a fast random walk algorithm is adapted to quadratic and cubic Koch boundaries in Sec. III, being particularly efficient due to their hierarchical geometry. The numerical results are described in Sec. IV.

II. MULTIFRACTAL EXPONENTS

Let us consider, for a given scale δ, a convenient cover of the studied boundary $\mathcal{S}$ by a finite number of disjoint compact sets $\{\Gamma_k^{(\delta)}\}$ (spheres, cubes, etc.) with diameter δ. The harmonic measure ω can be represented by the probabilities

$$p_{k,\delta}=\omega\{\mathcal{S}\cap\Gamma_k^{(\delta)}\}$$

that the Brownian motion is absorbed on the kth element of the boundary $\mathcal{S}$. For the sake of simplicity, we consider such a cover that all $p_{k,\delta}$ are strictly positive. The measure normalization condition holds whatever δ,

$$\sum_k p_{k,\delta}=1. \tag{1}$$

The numbers $p_{k,\delta}$ can thus be thought as a probability distribution characterized by its moments:

$$\zeta(q,\delta)=\sum_k (p_{k,\delta})^q \quad (q\in\mathbb{R}).$$

Changing the scale parameter δ, one studies how the moments of this distribution vary. Dealing with harmonic mea-

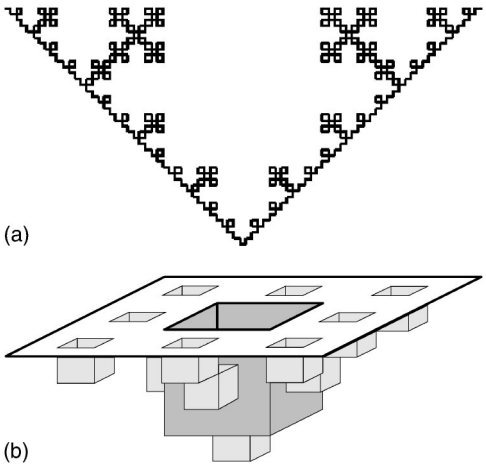

FIG. 1. Quadratic and cubic concave Koch boundaries with Hausdorff dimensions $D_0=\ln 5/\ln 3$ and $D_0=\ln 13/\ln 3$, respectively.

*Electronic address: denis.grebenkov@polytechnique.edu

sure on regular fractals (e.g., iterative self-similar fractals), one finds a power law:

$$\zeta(q,\delta) \sim \delta^{\tau(q)}$$

where $\tau(q)$ are called multifractal exponents. These exponents characterize the scaling (multifractal) properties of the harmonic measure. One also considers the multifractal dimensions:

$$D_q = \frac{\tau(q)}{q-1}.$$

Since it is not possible to study numerically infinite fractals, one has to introduce *local multifractal exponents* $\tau(q,\delta)$ which can be considered as approximations of the multifractal exponents $\tau(q)$ on a given finite generation of the fractal:

$$\tau(q,\delta) = \frac{\ln\zeta(q,\delta)}{\ln\delta}, \quad \tau(q) = \lim_{\delta\to 0}\tau(q,\delta). \tag{2}$$

In order to proceed to the limit $\delta\to 0$, one needs to calculate the moments $\zeta(q,\delta)$ for any positive δ. At the same time, the scales δ should be larger than the smallest length ℓ of a finite generation (minimal cutoff) which is chosen for the calculation. Indeed, if one takes the limit $\delta\to 0$ for a *finite* generation, the calculated values of $\tau(q,\delta)$ will converge to the multifractal exponents of the harmonic measure on a linear segment: $\tau_0(q)=q-1$. This trivial result has no interest. Consequently, one should deal with scales δ lying between the smallest length ℓ and the diameter $L=1$ of the whole boundary. In other words, the limit $\delta\to 0$ should be taken for increasing generations of the fractal in order to keep the inequality $\delta \geqslant \ell$. In practice, however, the numerical simulations can be carried out only for several first generations of the fractal.

This difficulty appears in all topics related to the numerical multifractal analysis. In fact, one typically observes a slow convergence of the local multifractal exponents $\tau(q,\delta)$ to their limiting values. Consequently, these local exponents given by numerical simulations for several generations of the fractal cannot be considered as good approximations for the multifractal exponents $\tau(q)$ on a really fractal boundary (infinite generation).

In this paper, we propose a useful *logarithmic development* for the local multifractal exponents. First, we consider a smooth boundary in the d-dimensional space. In this case, the harmonic measure defined on the boundary can be characterized by its density $\omega(s)$, i.e., the harmonic measure of an infinitesimal vicinity of the boundary point s is proportional to its surface area ds with coefficient $\omega(s)$ depending on s. Whatever the cover $\{\Gamma_k^{(\delta)}\}$ used with sufficiently small δ, the probabilities $p_{k,\delta}$ can be written as $p_{k,\delta}\simeq\delta^{d-1}\omega(s_k)$, where δ^{d-1} represents the surface area of the corresponding boundary element containing the boundary point s_k. The moments $\zeta(q,\delta)$ of this distribution are

$$\zeta(q,\delta) = \sum_k p_{k,\delta}^q \simeq \delta^{(d-1)(q-1)}\sum_k \omega^q(s_k)\,\delta^{d-1}.$$

The last sum can be written as the Riemann integral over the surface $\mathcal{S}$:

$$\zeta(q,\delta) = \delta^{(d-1)(q-1)}\left(\int_{\mathcal{S}}\omega^q(s)ds + O(\delta)\right),$$

where the correction term $O(\delta)$ is at least of order of δ. Consequently, the local multifractal exponents in the case of a smooth boundary are given as

$$\tau(q,\delta) = (d-1)(q-1) + \frac{\ln\int_{\mathcal{S}}\omega^q(s)ds}{\ln\delta} + O\left(\frac{\delta}{\ln\delta}\right). \tag{3}$$

The first term can be easily identified as the multifractal exponent $\tau(q)$ of the harmonic measure on a smooth boundary (of dimension $d-1$). The second term is responsible for a slow logarithmic decrease of the local multifractal exponents $\tau(q,\delta)$ to their limiting values $\tau(q)$. The third term accounts other possible corrections.

Being defined on fractals, the harmonic measure cannot be characterized by a density function, and the previous analysis falls down. However, the relation (3) may be useful even in this case. In fact, we propose a *conjectural* extension of the logarithmic development for the local multifractal exponents $\tau(q,\delta)$:

$$\tau(q,\delta) = \tau(q) + \frac{\tau_{\log}(q)}{\ln\delta} + O\left(\frac{\delta^{\eta_q}}{\ln\delta}\right), \tag{4}$$

where the first term presents the multifractal exponent of the harmonic measure, the second term provides a slow logarithmic decrease with a coefficient $\tau_{\log}(q)$, and the third term vanishes rapidly as a certain power η_q of the scale δ. Dealing with a finite generation of the fractal, the minimal scale value δ is equal to the smallest segment length ℓ, which decreases exponentially with the order of generation g **(**e.g., $\ell_g=(1/3)^g$ for the quadratic Koch curve, see below**)**. It means that the correction term in Eq. (4) vanishes *exponentially* with increasing generation order.

For practical purposes, this result has a very important meaning. Using the logarithmic development (4) without a correction term, one requires just two values of the local multifractal exponents, $\tau(q,\delta)$ and $\tau(q,\delta')$, in order to find the multifractal exponent $\tau(q)$: first, one calculates the coefficient $\tau_{\log}(q)$,

$$\tau_{\log}(q) \simeq \frac{\tau(q,\delta)-\tau(q,\delta')}{1/\ln\delta - 1/\ln\delta'},$$

second, one obtains the multifractal exponent $\tau(q)$,

$$\tau(q) \simeq \tau(q,\delta) - \frac{\tau_{\log}(q)}{\ln\delta}.$$

If one disposes of several values of local multifractal exponents for different scales, an extrapolation method can be applied in order to obtain $\tau_{\log}(q)$ and $\tau(q)$ with high accu-

racy. In summary, the use of the conjectural logarithmic development (4) allows one to calculate the multifractal exponents of the harmonic measure on a fractal boundary by computing only on its first generations.

A similar analysis can be carried out for the particular case of the local information dimension $D_{1,\delta}$ related to the entropy $\zeta_{ent}(\delta)$:

$$D_{1,\delta} = \lim_{q\to 1} \frac{\tau(q,\delta)}{q-1} = \frac{\zeta_{ent}(\delta)}{\ln 1/\delta},$$

$$\zeta_{ent}(\delta) = -\sum_k p_{k,\delta} \ln p_{k,\delta}.$$

In this case, the logarithmic development for the local information dimension $D_{1,\delta}$ can be written as

$$D_{1,\delta} = D_1 + \frac{D_{1,\log}}{\ln 1/\delta} + O\left(\frac{\delta^{\eta_1}}{\ln \delta}\right). \tag{5}$$

As previously, it allows one to compute the information dimension D_1 using only the first generations.

Finally, these concepts can be extended to an accurate calculation of the *multifractal spectrum* $f(\alpha)$ defined as Legendre transform of the multifractal exponents $\tau(q)$:

$$f(\alpha) = \min_q \{q\alpha - \tau(q)\}.$$

For a regular fractal $\mathcal{S}$, it has been shown that $f(\alpha)$ gives the Hausdorff dimension of a subset of $\mathcal{S}$ where the harmonic measure scales with exponent α [6,7].

Since the preceding analysis concerning only the scale δ is guessed to be valid for any (positive) q, it can be applied to compute the multifractal spectrum $f(\alpha)$. First, one uses the analyticity of the multifractal exponents $\tau(q)$ to write the Legendre transform in a parametric form:

$$\alpha_q = \frac{d\tau(q)}{dq}, \quad f(\alpha_q) = q\alpha_q - \tau(q).$$

For numerical computation, one introduces the local analogs $\alpha_q(\delta)$ and $f(\alpha_q(\delta),\delta)$ which depend on the scale δ, and converge, respectively, to α_q and $f(\alpha_q)$ as $\delta\to 0$:

$$\alpha_q(\delta) = \frac{d\tau(q,\delta)}{dq}, \quad f(\alpha_q,\delta) = q\alpha_q(\delta) - \tau(q,\delta).$$

The substitution of the logarithmic development for the local multifractal exponents $\tau(q,\delta)$ into these relations leads to a similar development for the multifractal spectrum:

$$\alpha_q(\delta) = \alpha_q + \frac{\alpha_{q,\log}}{\ln \delta} + O\left(\frac{\delta^{\kappa_q}}{\ln \delta}\right),$$

$$f(\alpha_q(\delta),\delta) = f(\alpha_q) + \frac{f_{q,\log}}{\ln \delta} + O\left(\frac{\delta^{\mu_q}}{\ln \delta}\right), \tag{6}$$

where the last terms vanish rapidly as $\delta\to 0$. Again, it is sufficient to use the first generations to calculate the multifractal spectrum with high accuracy. Note also that the present approach is not specifically restricted to the harmonic measure as it can be applied for the multifractal analysis of other measures.

In the following sections, we apply the logarithmic development for the local multifractal exponents in order to compute the multifractal dimensions of the harmonic measure on the quadratic and cubic Koch boundaries. These results can be considered as a numerical verification of the above mathematical conjecture.

III. GEOMETRY-ADAPTED FAST RANDOM WALK ALGORITHM

Except a few particular cases, the harmonic measure cannot be calculated in an analytical way. Among various numerical methods, one frequently chooses the Monte Carlo simulations which can be roughly divided into two groups called "on-lattice" and "off-lattice." In the first case, one introduces a convenient lattice with mesh $a \leqslant \delta$ in order to discretize the bulk (e.g., square or cubic lattice). Lattice cells provide convenient cover $\{\Gamma_k^{(\delta)}\}$ of the boundary $\mathcal{S}$. The Brownian motion is then modeled by random walks moving on the lattice and absorbed by the surface. Launching random walkers from a fixed lattice point x_0, one calculates the frequencies of absorptions on different boundary elements. In the limit when the number of random walkers N goes to infinity, the distribution of these frequencies converges to the distribution $\{p_{k,\delta}\}$ representing the harmonic measure on the scale δ. The "on-lattice" approaches can be easily realized for various domains, but they are efficient, in general, only for simple geometries. Dealing with fractal shapes, one should keep the lattice mesh a smaller than the smallest geometrical feature length (minimal cutoff). If the distance between the starting point x_0 and the absorbing boundary $\mathcal{S}$ is of order of its diameter L, the numerical simulations of random trajectories from x_0 to $\mathcal{S}$ become very long and time-consuming.

In "off-lattice" approaches, one replaces long random walk trajectories by a sequence of random jumps of different lengths. For the diffusing particle started from a given point x_0, one first determines the distance d_0 between x_0 and the absorbing boundary $\mathcal{S}$. Then the disk B_0 of radius d_0, centered at x_0, does not contain any "obstacle" for the random particle. Thanks to the continuity of the Brownian motion, it should intersect the corresponding circle before the absorption on the boundary $\mathcal{S}$. Rotational symmetry implies that the distribution of intersection points is uniform. It means that one can replace the complex Brownian motion trajectory inside the disk B_0 by a random jump from x_0 to a uniformly distributed point x_1 on its boundary (circle). Starting now from x_1, one calculates the distance d_1 between x_1 and $\mathcal{S}$, considers the disk B_1 of radius d_1, and chooses uniformly a random point x_2 on its boundary. This procedure provides a sequence of random points $\{x_n\}$ on a Brownian trajectory. When a new random point x_n becomes closer to the surface $\mathcal{S}$ than a chosen threshold value, one terminates the simulation saying that the random particle is absorbed on the boundary element nearest to the current point x_n. Repeating these simulations many times, one obtains the distribution of frequencies of absorptions on different boundary elements. The es-

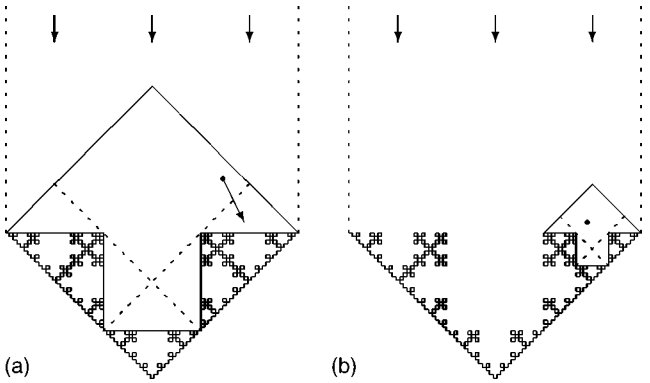

FIG. 2. The basic arrowlike cell is divided into the rotated square and five small triangles (a). Once the Brownian particle arrived into the rotated square (level 1), the distance between its current position (full circle) and the boundary can be estimated explicitly. It allows one to execute random jumps inside the rotated square until the Brownian particle exits from the arrowlike cell (passage to level 0), or enters into a small triangle (passage to level 2). In the last case, the Brownian particle can "see" the geometrical details of the next generation. The rescaled arrowlike cell (b) can be thus used to estimate the distance between the current particle position (full circle) and the boundary. Note that a distant source is placed on the top of the figure, while two vertical borders with periodic conditions are drawn by dotted lines.

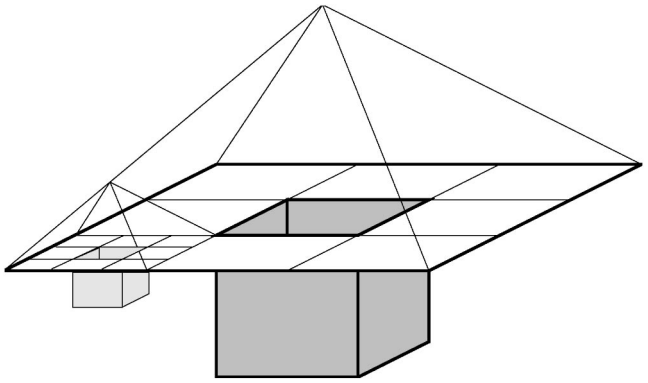

FIG. 3. First generation of the cubic Koch surface. The three-dimensional cell is composed of the pyramid (of square base $L \times L$ and of height $L/2$) and small cube (with edge $L/3$). This cell is divided onto 13 smaller cells and the rest volume.

sential advantage of the "off-lattice" approach is that each random jump is made on the maximum possible distance. This method is valid to model the Brownian motion for any dimension of the embedding space (if the disks B_n are replaced by d-dimensional spheres).

The main difficulty of this fast random walk algorithm is to determine the distance between a given point x and the boundary $\mathcal{S}$ which has no analytic expression except a few particular cases. In the general situation, the numerical determination of the distance can be even more time-consuming than the realization of long random trajectories in "on-lattice" approaches.

The idea of the coarse maps technique developed by Ossadnik to study diffusion-limited aggregation (DLA) [8] becomes particularly efficient for self-similar Koch type geometries. One can use the fact that any generation of the quadratic Koch curve is "enclosed" to the next one. When a random walker is far from the surface $\mathcal{S}$, it cannot distinguish its geometrical features. Consequently, the length of the random jump can be taken as the distance between the current point and the generation zero (horizontal segment). Getting closer and closer to the boundary, the random walker can recognize smaller and smaller geometrical details. One should then use finer and finer calculation of the jump length. The key point here is that the random walker being near a small part of the boundary cannot "see" the rest of the boundary. Consequently, one can determine the jump length examining only the *local* geometrical environment.

In order to clarify these ideas, we are going to follow a possible trajectory of the random particle from a distant source to the generation g of the quadratic Koch curve.

(1) **Level** 0. The Brownian motion begins from a distant source. While the current position x_n of the Brownian particle is far from the boundary $\mathcal{S}_g$, the random jump length can be taken to be equal to the distance between x_n and $\mathcal{S}_0$, i.e., to the height of the particle position above the horizontal segment (Fig. 2). Note that the periodic boundary condition is imposed on the vertical borders: if the particle ought to be placed to the left of the left border, it appears at a corre-

TABLE I. Entropy $\zeta_{ent}(\delta)$ of the distribution $\{p_{k,\delta}\}$ for the first ten generations of the quadratic Koch curve on different scales δ.

δ/g	1	2	3	4	5	6	7	8	9	10
$(1/3)$	1.2571	1.2653	1.2682	1.2693	1.2697	1.2699	1.2699	1.2699	1.2699	1.2699
$(1/3)^2$		2.3829	2.3950	2.3995	2.4012	2.4018	2.4020	2.4021	2.4021	2.4021
$(1/3)^3$			3.4851	3.4988	3.5039	3.5058	3.5065	3.5068	3.5069	3.5069
$(1/3)^4$				4.5840	4.5982	4.6036	4.6056	4.6063	4.6066	4.6067
$(1/3)^5$					5.6825	5.6970	5.7024	5.7045	5.7052	5.7055
$(1/3)^6$						6.7811	6.7956	6.8011	6.8031	6.8039
$(1/3)^7$							7.8797	7.8942	7.8997	7.9018
$(1/3)^8$								8.9783	8.9928	8.9983
$(1/3)^9$									10.0768	10.0914
$(1/3)^{10}$										11.1755

TABLE II. Local information dimension D_{1,ℓ_g} for different generations g of the quadratic Koch fractal on the smallest scale $\ell_g=(1/3)^g$.

g	1	2	3	4	5	6	7	8	9	10
D_{1,ℓ_g}	1.1442	1.0845	1.0574	1.0431	1.0345	1.0287	1.0246	1.0215	1.0191	1.0172

sponding position near the right border, and vice versa.

(2) **Level** 1. When the Brownian particle approaches the boundary $\mathcal{S}_g$, it can enter the arrowlike cell composed of five small triangles and the rotated square [Fig. 2(a)]. If the Brownian particle falls at once into a small triangle, one passes directly to the level 2. For the particle arrived to the rotated square, the random jump length is taken to be equal to the distance between x_n and the first generation $\mathcal{S}_1$ that can be calculated explicitly. Such a random jump can either change the position of the Brownian particle inside the rotated square (then one recalculates the distance and executes a new jump), or bring it out of the arrowlike cell (then one returns to the level 0), or move it into one of the small triangles (then one passes to the level 2).

(3) **Level** 2. The small triangle can be seen as a coarse-grained form of a similar allowlike cell scaled by factor 1/3 [Fig. 2(b)]. When the Brownian particle falls into this triangle, it can "see" the details of the allowlike cell that is composed of five small triangles and the rotated square. Again, the random jumps inside the rotated square can either change the particle's position or bring out to level 1 or 3, and so on.

(4) **Level** g. When the Brownian particle reaches the last level g (i.e., the chosen generation of the fractal boundary), it moves inside the corresponding arrowlike cell until one of two events: either it brings out of this level onto the previous level (and the motion continues), or it approaches the boundary $\mathcal{S}_g$ (which coincides with $\mathcal{S}_1$ at this scale) by a distance less than a chosen threshold value. In this case, the Brownian particle is considered as being absorbed.

Based on particular features of self-similar Koch geometries, this numerical method can be called the *geometry-adapted fast random walk* (GAFRW) algorithm.

The three-dimensional case can be treated in a similar way. One considers a three-dimensional arrowlike cell composed of the square pyramid and small cube (see Fig. 3). This cell can be divided onto 13 smaller pyramids and the rest volume. When the Brownian particle started from a distant source enters into the arrowlike cell, there are three possibilities: to leave this cell (level 0), to stay at this cell (level 1), and to enter into one of the small pyramids (level 2), and so on. Once again, one takes advantage of the deterministic hierarchical structure of the boundary to speed up the random walk simulations.

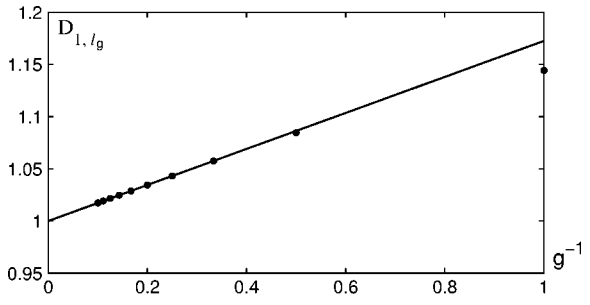

FIG. 4. Dependence of the local information dimension D_{1,ℓ_g} on the generation order g. An extrapolation of these data (see Table II), for g lying between 4 and 10, provides $D_1=1.0000$. A remarkable agreement with logarithmic development can be observed even for the second generation.

IV. NUMERICAL RESULTS

A. Quadratic Koch curve

We consider the first ten generations of the self-similar quadratic Koch curve with Hausdorff dimension $D_0=\ln 5/\ln 3\approx 1.4650$. Using the GAFRW algorithm, we calculate the distribution of frequencies of absorptions on boundary elements $\mathcal{S}\cap\Gamma_k^{(\delta)}$ of the curve on different scales δ. When the number of random particles N goes to infinity, this distribution converges to the distribution $\{p_{k,\delta}\}$ of hitting probabilities on different scales δ. Using a large but finite number N, one obtains an approximation of this distribution. It is known that the relative error of such approximation decreases slowly, as $N^{-1/2}$. Although an accurate computation of small probabilities (like 10^{-10}) would require a huge number of simulations, the contribution of these probabilities to the average characteristics of the harmonic measure **(**like entropy $\zeta_{ent}(\delta)$ or second moment $\zeta(2,\delta)$**)** are completely negligible. Consequently, one can calculate these characteristics very accurately by using a reasonable number of random particles. At the same time, this reasoning falls down for the moments $\zeta(q,\delta)$ of negative orders $(q<0)$, where the contribution of small probabilities dominates. In what follows, we focus our attention on positive order moments $\zeta(q,\delta)$ and entropy $\zeta_{ent}(\delta)$.

In order to estimate the accuracy of our calculations, we perform ten series of simulations for each generation, using

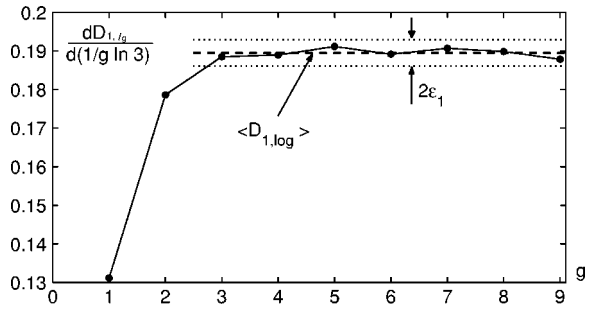

FIG. 5. The derivative $dD_{1,\ell_g}/d(1/g\ln 3)$ as a function of g becomes constant from $g=3$. This allows one to derive the mean coefficient $\langle D_{1,\log}\rangle$ and the double maximum deviation ε_1.

TABLE III. Moments $\zeta(2,\delta)$ of the distribution $\{p_{k,\delta}\}$ for the first ten generations of the quadratic Koch curve on different scales δ. The last column contains the factor which should be multiplied to the values in the corresponding line.

δ/g	1	2	3	4	5	6	7	8	9	10	
$(1/3)$	3.2774	3.2496	3.2397	3.2361	3.2347	3.2342	3.2340	3.2340	3.2339	3.2339	$\times 10^{-1}$
$(1/3)^2$		1.1820	1.1688	1.1638	1.1620	1.1613	1.1611	1.1609	1.1609	1.1609	$\times 10^{-1}$
$(1/3)^3$			4.3935	4.3403	4.3201	4.3126	4.3099	4.3087	4.3083	4.3082	$\times 10^{-2}$
$(1/3)^4$				1.6450	1.6246	1.6168	1.6139	1.6128	1.6124	1.6123	$\times 10^{-2}$
$(1/3)^5$					6.1687	6.0915	6.0623	6.0510	6.0471	6.0455	$\times 10^{-3}$
$(1/3)^6$						2.3139	2.2849	2.2739	2.2698	2.2682	$\times 10^{-3}$
$(1/3)^7$							8.6805	8.5715	8.5301	8.5145	$\times 10^{-4}$
$(1/3)^8$								3.2563	3.2155	3.2000	$\times 10^{-4}$
$(1/3)^9$									1.2216	1.2063	$\times 10^{-4}$
$(1/3)^{10}$										4.5828	$\times 10^{-5}$

10^9 random particles in each case. Since these simulations are independent, fluctuations of computed values will indicate the corresponding stochastic error. For all local information dimensions D_{1,ℓ_g} and local correlation exponents $\tau(2,\ell_g)$, the observed fluctuation is less than 10^{-5}, i.e., all five significant digits, shown in Tables II, IV, VIII, and X, are correct.

Once the local exponents are computed for different finite order generations, one uses the logarithmic development to calculate the multifractal exponents corresponding to the mathematical fractal of infinite order. For the finite generations of sufficiently high order, the correction terms in the logarithmic development can be neglected. An extrapolation of the local exponents provides then an accurate computation of the corresponding multifractal exponents.

1. Information dimension

The entropy $\zeta_{ent}(\delta)$ is computed on different scales δ between $1/3$ and $\ell_g=(1/3)^g$ (Table I). Comparing its values for different generations on the same scale δ (in a line), one finds that these entropies rapidly approach a stable value which does not vary with further increase of the generation order g. It means that, for a given scale δ, the appearance of new irregularities on smaller scales almost does not change the entropy on the scale δ. One will see that this result is general for other moments of positive orders. Roughly speaking, if we are not interested in the scaling behavior of the harmonic measure on the scales smaller than δ, it does not matter if one deals with the moderate generation of order of $\ln\delta/\ln(1/3)$, with any extremely high generation, or with a real mathematical fractal of infinite order.

Taking values on the diagonal of Table I which correspond to the smallest scale $\delta=\ell_g$ for a given generation order g, one calculates the local information dimension D_{1,ℓ_g} (Table II). One remarks a slow monotonic decrease of these numbers. Writing the logarithmic development (5) as

$$D_{1,\ell_g} \simeq D_1 + \frac{1}{g}\frac{D_{1,\log}}{\ln 3} \tag{7}$$

one can derive from the extrapolation method described below the information dimension D_1 with high accuracy (see the next section for estimation of the error bars):

$$D_1 = 1.0000 \pm 0.0003. \tag{8}$$

This numerical value is remarkably close to its theoretical value $D_1=1$ predicted by Makarov's theorem [3]. This excellent agreement supports the conjectural logarithmic development (5) and the efficiency of the method on the whole. The linear dependence (7) of the local information dimensions D_{1,ℓ_g} on $1/g$ is satisfied even from the second generation as shown in Fig. 4.

2. Accounting for systematic errors

The use of the logarithmic development without correction term leads to systematic errors that have to be accounted for. The accuracy of the limiting values of the multifractal exponents is essentially determined by the accuracy of computation of the coefficient $D_{1,\log}$ in front of the logarithmic term. For these purposes, we compute numerically the derivative $dD_{1,\ell_g}/d(1/g\ln 3)$ that provides an approximation to $D_{1,\log}$ according to the logarithmic development, up to the correction term that vanishes rapidly with the generation order g. The dependency of this derivative on g is shown in Fig. 5. One recognizes that it is almost constant from $g=3$,

TABLE IV. Local correlation exponent $\tau(2,\ell_g)$ for different generations g of the quadratic Koch fractal on the smallest scale $\ell_g=(1/3)^g$.

g	1	2	3	4	5	6	7	8	9	10
$\tau(2,\ell_g)$	1.0154	0.9719	0.9482	0.9347	0.9263	0.9207	0.9166	0.9136	0.9113	0.9094

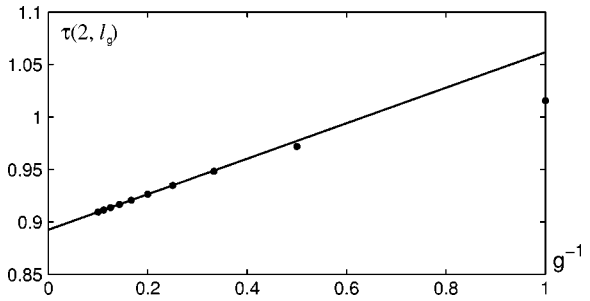

FIG. 6. Dependence of the local correlation exponent $\tau(2,\ell_g)$ on the generation order g. An extrapolation of these data (see Table IV), for g lying between 4 and 10, provides $\tau(2)=0.8925$. A very good agreement with logarithmic development can be observed even for the third generation.

up to the fluctuations due to systematic errors. One can thus compute the mean value of $D_{1,\log}$ and the double maximum deviation ε_1 from this mean:

$$\varepsilon_1 = 2 \max_{3\leqslant g\leqslant 9} \left| \frac{dD_{1,\ell_g}}{d(1/g \ln 3)} - \langle D_{1,\log}\rangle \right|.$$

The limiting value of the information dimension D_1 lies thus in the confidence interval $[D_1^-, D_1^+]$, where

$$D_1^{\pm} = \left(D_{1,\ell_g} - \frac{1}{g}\frac{\langle D_{1,\log}\rangle}{\ln 3} \right) \pm \frac{1}{g}\frac{\varepsilon_1}{\ln 3},$$

g being the maximum generation order available for the numerical simulations.

This scheme has been applied throughout this paper to account for the systematic errors for other multifractal dimensions, both in the two- and three-dimensional cases.

3. Correlation dimension

Similarly, one can study any positive moment $\zeta(q,\delta)$ of the probability distribution $\{p_{k,\delta}\}$ for different generation orders g and scales δ. The correlation dimension $D_2=\tau(2)$ is particularly important for the Laplacian transfer phenomena [9,10]. Table III shows the moments $\zeta(2,\delta)$ on different scales δ between $1/3$ and $\ell_g=(1/3)^g$.

Again, taking the values on the diagonal of Table III which correspond to the smallest scale $\delta=\ell_g$ for a given generation order g, one calculates the local multifractal exponents $\tau(2,\ell_g)$ (Table IV). With the help of the logarithmic development (4) written as

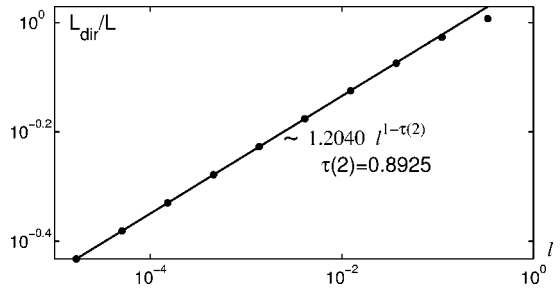

FIG. 7. Dirichlet active zone lengths for the first ten generations of the quadratic Koch curve. As described, these lengths follow a power law with exponent $1-\tau(2)$, with $\tau(2)=0.8925$.

$$\tau(q,\ell_g) \simeq \tau(q) + \frac{1}{g}\frac{\tau_{\log}(q)}{\ln 1/3} \tag{9}$$

the correlation exponent can be deduced from the extrapolation method described above:

$$\tau(2) = 0.8925 \pm 0.0007. \tag{10}$$

Figure 6 shows that the linear dependence (9) of the local correlation exponents $\tau(2,\ell_g)$ on $1/g$ holds even from the third generation providing a good numerical verification for the logarithmic development.

4. Dirichlet active zone lengths

The data of Table III allow direct calculations of the Dirichlet active zone lengths [4,11,12] which are defined as the inverse of the second moment of the harmonic measure:

$$L_{act} = \frac{\ell}{\zeta(2,\ell)},$$

where ℓ is the smallest length of the chosen generation. Taking the values of the second moments $\zeta(2,\delta)$ on the diagonal of Table III, one obtains the Dirichlet active zone lengths given in Table V. One remarks the slow decrease of these lengths when the generation order g increases. Figure 7 shows that this length follows a power law $L_{act}\sim\ell^{1-\tau(2)}$.

Note that the Dirichlet active zone length characterizes the asymptotic behavior of the spectroscopic impedance in the limit of high frequencies [12].

5. Box-counting method

The obtained data allow one to check another method frequently used to calculate the multifractal dimensions. Within this *box-counting method*, one fixes the highest generation available for a chosen numerical method and calculates the moments $\zeta(q,\delta)$ on different scales δ. For the qua-

TABLE V. Dirichlet active zone lengths for the first ten generations of the quadratic Koch curve. These lengths vary slowly as $L_{act}\sim\ell^{1-\tau(2)}$. The corresponding perimeters are given for comparison.

g	1	2	3	4	5	6	7	8	9	10
L_{act}	1.0171	0.9400	0.8430	0.7505	0.6671	0.5928	0.5268	0.4681	0.4159	0.3695
L_{tot}	1.67	2.78	4.63	7.72	12.86	21.43	35.72	59.54	99.23	165.38

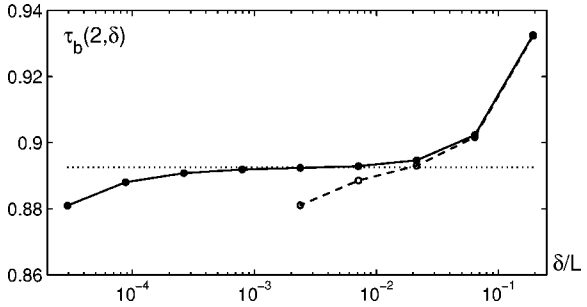

FIG. 8. Numerical values of the correlation exponent $\tau_b(2,\delta)$ given by the box-counting method for generation orders $g=6$ (dashed line) and $g=10$ (solid line). The straight dotted line represents the value $\tau(2)=0.8925$ obtained with the help of the logarithmic development (4).

dratic Koch curve, these results are shown in the last column of Table III. The logarithmic derivatives of the moments $\zeta(q,\delta)$ with respect to δ provide the numerical estimates $\tau_b(q,\delta)$ of the multifractal exponents for finite δ:

$$\tau_b(q,\delta) = \frac{\partial \ln \zeta(q,\delta)}{\partial \ln \delta}.$$

For a numerical computation, one takes two close values δ' and δ'' in order to approximate this logarithmic derivative as

$$\tau_b(q,\delta) \approx \frac{\ln \zeta(q,\delta') - \ln \zeta(q,\delta'')}{\ln \delta' - \ln \delta''}, \quad \delta \approx \sqrt{\delta' \delta''}.$$

In particular, the variation of the box-counting correlation exponent $\tau_b(2,\delta)$ with δ is shown in Fig. 8.

One finds a good agreement between these values and $\tau(2)=0.8925$ obtained previously. The decrease of $\tau_b(2,\delta)$ for small δ corresponds to the use of finite generations: at the minimal cutoff ℓ_g, one replaces the infinite self-similar fractal by a linear segment. On the other hand, the increase of $\tau_b(2,\delta)$ for large δ is caused by the fact that the fractality is not yet well-established on such scales.

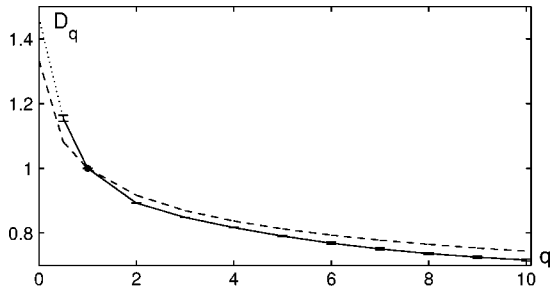

FIG. 9. Multifractal dimensions D_q of the harmonic measure on the quadratic Koch curve (solid line) and on two-dimensional percolation clusters (dashed line). The intersection point is guaranteed by the Makarov's theorem. The error bars are always smaller than 3×10^{-3}. The largest error is obtained for smaller order. The region of orders q around 0 is shown by a dotted line since the error bars become too large.

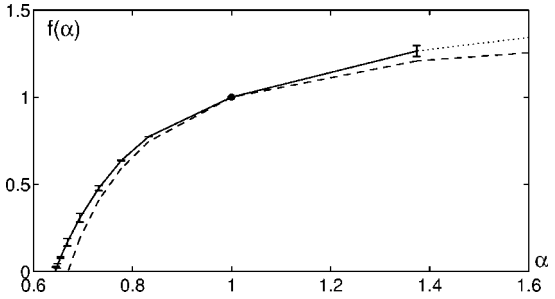

FIG. 10. Multifractal spectrum $f(\alpha)$ of the harmonic measure on the quadratic Koch curve (solid line) and on two-dimensional percolation clusters (dashed line). The intersection point corresponds to the Makarov's theorem. The error bars are always smaller than 3×10^{-2}. The largest error is obtained for smaller order.

In order to obtain a reasonable accuracy by the classical box-counting method (look at the "stabilization" for the tenth generation in Fig. 8), one has to consider high generations. In other words, the level corresponding to the value $\tau(2)=0.8925$ is not well-established for lower generations. It means that the use of this approach for low order generations (e.g., $g=6$) does not lead to an accurate determination of the multifractal exponents. It perhaps explains the values between 0.92 and 0.96 found in the literature for the correlation exponent $\tau(2)$ of the harmonic measure on similar Koch curves [13–15]. On the other hand, the logarithmic development provides very accurate results even for the first several generations (see Fig. 6).

6. Other dimensions and multifractal spectrum

In a similar way, one can calculate the other multifractal dimensions D_q. For the quadratic Koch curve, their dependency on the order q is shown in Fig. 9 (see [10] for numerical values). Multifractal spectra have already been computed in the literature for DLA aggregates [18,19] or percolation clusters [16,17]. For comparison, we draw on the same plot the multifractal dimensions as a function of q for two-dimensional percolation clusters obtained analytically by Duplantier. These two curves have an intersection at point $q=1$ since the information dimension in both cases is equal to 1 according to the Makarov's theorem. This result constitutes the first accurate comparison of the multifractal dimensions for both deterministic and stochastic boundaries.

The multifractal spectrum $f(\alpha)$ of the harmonic measure on the quadratic Koch curve has been numerically computed for the first time by Evertsz and Mandelbrot for the first generations [20]. The GAFRW algorithm allows one to reproduce this study for higher generations, while the logarithmic development (6) improves its accuracy. Figure 10 shows the left-hand side part of this spectrum that corresponds to

TABLE VI. Number of random particles N used to realize the GAFRW algorithm.

g	1	2	3	4	5	6
N	1.2×10^9	9×10^8	5×10^9	1.5×10^{10}	1.6×10^{10}	5×10^{10}

TABLE VII. Entropy $\zeta_{ent}(\delta)$ of the distribution $\{p_{k,\delta}\}$ for the first six generations of the cubic Koch surface on different scales δ.

δ/g	1	2	3	4	5	6
$(1/3)$	2.2867	2.2878	2.2882	2.2883	2.2884	2.2884
$(1/3)^2$		4.5195	4.5209	4.5215	4.5218	4.5218
$(1/3)^3$			6.7320	6.7336	6.7343	6.7345
$(1/3)^4$				8.9386	8.9402	8.9409
$(1/3)^5$					11.143	11.145
$(1/3)^6$						13.347

positive moments. For comparison, we draw the multifractal spectrum for two-dimensional percolation clusters. Although the deterministic Koch curve and random percolation clusters present very different geometries, the left hand sides of their multifractal spectra are relatively close to each other. In other words, the multifractal dimensions of the harmonic measure corresponding to positive moments are not very sensitive to the particular distribution of highly accessible boundary points. On the other hand, these dimensions may be more specific of the geometry in the region of negative moments hence the two curves should exhibit larger differences.

At the same time, the region of negative moments, which corresponds to the right-hand side of the multifractal spectrum, is much more difficult to compute accurately. This right-hand side is mostly determined by the values of the harmonic measure on the boundary points of low accessibility and the numerical method used in this paper loses most of its interest.

B. Cubic Koch surface

Similar numerical simulations are carried out for the first six generations of the self-similar cubic Koch surface with Hausdorff dimension $D_0=\ln 13/\ln 3\approx 2.3347$. Again, one uses the geometry-adapted fast random walk algorithm in order to calculate the distribution of frequencies of absorptions on boundary elements $\mathcal{S}\cap\Gamma_k^{(\delta)}$ on different scales δ. For large N, this distribution provides a good approximation for the distribution $\{p_{k,\delta}\}$ of hitting probabilities on this surface on different scales δ. Table VI describes the number of random particles used for the calculation for each generation. As previously, one separates these simulations in ten groups in order to estimate stochastic errors, while the systematic errors are taken into account by our extrapolation method.

1. Information dimension

The calculation of the information dimension in the two-dimensional case has been realized as a verification test for our method since the Makarov's theorem provides the exact value $D_1=1$ for any simply connected set in the plane. The situation is drastically different in the three-dimensional case, where one can mention two important mathematical results:

(1) Bourgain's theorem states that the information dimension D_1 of the harmonic measure is strictly less than the space dimension d [21]; and

(2) Wolff's counterexample to a hypothetic extension of the Makarov's theorem to $\mathbb{R}^3$ shows that there exists a regular (e.g., self-similar) fractal for which the information dimension D_1 of the harmonic measure is strictly greater than 2 [22].

Consequently, there is no particular reason to obtain the information dimension being equal to 2.

In three dimensions, the numerical calculations are significantly more difficult to realize for high generation orders than in the planar case. The use of the GAFRW algorithm for the cubic Koch surface together with the logarithmic development allow one to calculate the information dimension accurately.

Table VII shows the entropy $\zeta_{ent}(\delta)$ on different scales δ between $1/3$ and $\ell_g=(1/3)^g$. Taking the values on the diagonal of Table VII, which correspond to the smallest scale $\ell_g=(1/3)^g$ for a given generation order g, one calculates the local information dimensions D_{1,ℓ_g} (see Table VIII). As previously, one notices a monotonic decrease of these numbers. Using the logarithmic development, one obtains the information dimension D_1 of the harmonic measure on the cubic Koch surface by the extrapolation method:

TABLE VIII. Local information dimension D_{1,ℓ_g} for different generations of the cubic Koch surface on the smallest scale $\ell_g=(1/3)^g$.

g	1	2	3	4	5	6
D_{1,ℓ_g}	2.0814	2.0569	2.0426	2.0341	2.0286	2.0249

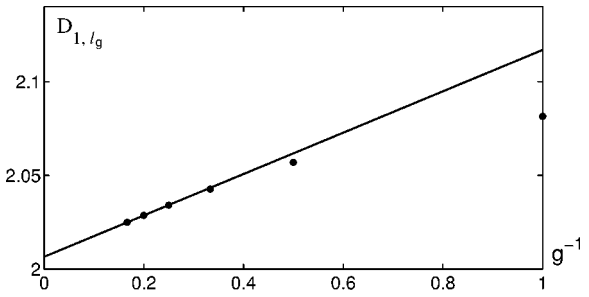

FIG. 11. Dependence of the local information dimensions D_{1,ℓ_g} on the generation order g. An extrapolation of these data (Table VIII), for g lying between 3 and 6, provides $D_1=2.007$.

TABLE IX. Moments $\zeta(2,\delta)$ of the distribution $\{p_{k,\delta}\}$ for the first six generations of the cubic Koch surface on different scales δ. The last column contains the factor which should be multiplied to the values in the corresponding line.

δ/g	1	2	3	4	5	6	
$(1/3)$	1.0952	1.0942	1.0938	1.0937	1.0936	1.0936	$\times 10^{-1}$
$(1/3)^2$		1.2245	1.2230	1.2224	1.2221	1.2220	$\times 10^{-2}$
$(1/3)^3$			1.3943	1.3925	1.3917	1.3914	$\times 10^{-3}$
$(1/3)^4$				1.6046	1.6025	1.6015	$\times 10^{-4}$
$(1/3)^5$					1.8570	1.8544	$\times 10^{-5}$
$(1/3)^6$						2.1552	$\times 10^{-6}$

TABLE X. Local correlation exponents $\tau(2,\ell_g)$ for different generations of the cubic Koch surface on the smallest scale $\ell_g = (1/3)^g$.

g	1	2	3	4	5	6
$\tau(2,\ell_g)$	2.0131	2.0037	1.9950	1.9883	1.9832	1.9794

$$D_1 = 2.007 \pm 0.002. \tag{11}$$

This value is very close to the information dimension 2 for a smooth boundary. According to the estimation scheme we used in this work, it seems to be possible to distinguish the obtained numerical value from 2. We emphasize again that, in three dimensions, there is no mathematical reason to expect a particular value for the information dimension (e.g., 2). On the other hand, the values 2.007 and 2 are impossible to distinguish in practice, for instance, in a physical experiment. Figure 11 shows that the linear dependence (7) holds from the third generation.

2. Correlation dimension and Dirichlet active zone areas

To study the correlation exponent $\tau(2)$, one computes the second moments $\zeta(2,\delta)$ given in Table IX, while Table X gives the local correlation exponents $\tau(2,\ell_g)$ corresponding to the diagonal elements. The logarithmic development provides the correlation exponent $\tau(2)$ by means of the extrapolation method:

$$\tau(2) = 1.963 \pm 0.006. \tag{12}$$

The linear dependence (9) of the local correlation exponents on $1/g$ is well satisfied from the third generation as shown in Fig. 12.

The Dirichlet active zone areas are computed as

$$S_{act} = \frac{\ell^2}{\zeta(2,\ell)}$$

and given in Table XI. One finds a slow decrease for increasing values of the generation order g.

3. Other dimensions and multifractal spectrum

In a similar way, one calculates the other multifractal dimensions D_q shown in Fig. 13 (see [10] for numerical values). After that, the logarithmic development (6) is used to determine the multifractal spectrum $f(\alpha)$ of the harmonic measure shown in Fig. 14.

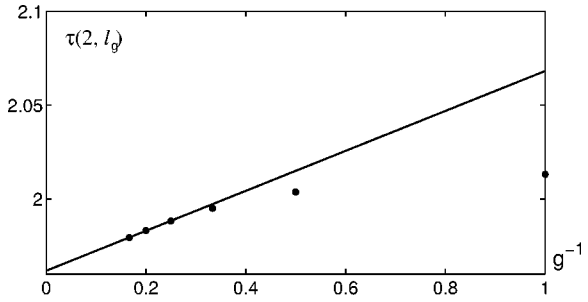

FIG. 12. Dependence of local correlation exponents $\tau(2,\ell_g)$ on the generation order g. An extrapolation of these data (Table X), for g lying between 3 and 6, provides $\tau(2)=1.963$.

TABLE XI. Dirichlet active zone areas for the first six generations of the cubic Koch surface. The total areas are given for comparison.

g	1	2	3	4	5	6
S_{act}	1.0145	1.0082	0.9838	0.9499	0.9120	0.8731
S_{tot}	1.4444	2.0864	3.0137	4.3531	6.2879	9.0825

V. CONCLUSIONS

In this paper we have studied the multifractal properties of the harmonic measure on quadratic and cubic Koch boundaries with Hausdorff dimensions $D_0 = \ln 5/\ln 3$ and $D_0 = \ln 13/\ln 3$. Applying the geometry-adapted fast random walk algorithm, we have calculated the distribution of hitting probabilities that represent the harmonic measure on a given scale δ. Dealing with the first ten generations of the quadratic Koch curve and with the first six generations of the cubic Koch surface, we have computed the local information and correlation dimensions, $D_{1,\delta}$ and $\tau(2,\delta)$, on different scales δ. In order to proceed the limit $\delta \to 0$, we have conjectured logarithmic developments (4) and (5) for the local multifractal exponents. The numerical data support the validity of this development. In particular, this result provides with high accuracy the multifractal dimensions D_1 and $\tau(2)$ of the harmonic measure on a really fractal boundary. Generally, use of this logarithmic development allows one to compute the multifractal exponents corresponding to the *infinite generation* dealing only with its first several generations.

An excellent agreement between the theoretical and numerical values of the information dimension in the two-dimensional case supports both the conjectural logarithmic development and our numerical method's applicability on the whole.

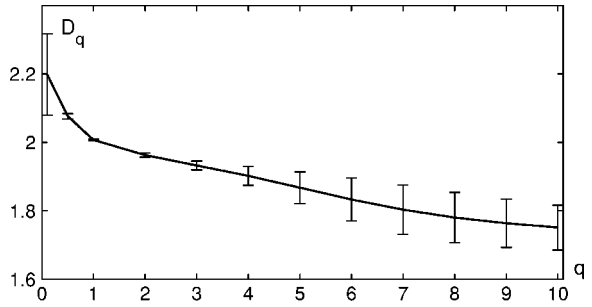

FIG. 13. Multifractal dimensions D_q of the harmonic measure on the cubic Koch surface. The error bar is large for $q \simeq 0$ since the contributions of small probabilities become more and more important. The error bars increase also for large q: the extrapolation method of Sec. IV A 2 is based on approaching to a constant value of the derivative $dD_{q,\ell_g}/d(1/g\ln 3)$ for a large generation order g. The first six generations used in this work are not sufficient to reach this value for large q.

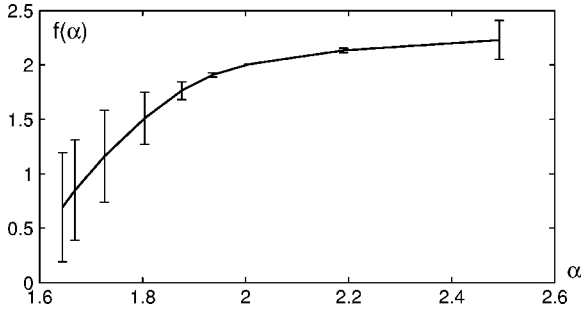

FIG. 14. Multifractal spectrum $f(\alpha)$ of the harmonic measure on the cubic Koch surface. The error bars increase when approaching the top of this $\cap$-shape ($q \simeq 0$) and also for small values of α (q going to infinity, see the caption of Fig. 13).

The determination of the information dimension D_1 of the harmonic measure on fractal surfaces in a general case remains an important problem. It has been solved analytically by Makarov for the two-dimensional case: $D_1 = 1$ for simply connected sets. The naive extension of this theorem onto the three-dimensional case is false. In particular, the information dimension of the harmonic measure defined on the regular (self-similar) fractal constructed by Wolff is strictly greater than 2. The information dimension for the cubic Koch surface is found to be equal to 2.007 ± 0.002 which seems to be the first accurate numerical computation of this important characteristic of the harmonic measure in three dimensions. It is striking that D_1 is very close to 2. In fact, it seems very difficult to exhibit strong deviations from this value. Finding surfaces with large D_1 presents a major challenge in these fields and could have strong practical applications.

For the correlation exponent $\tau(2)$, there is no analytical results providing an expected theoretical value. The obtained numerical value for the cubic Koch surface 1.963 ± 0.006 shows that this correlation exponent is relatively close to 2 (correlation exponent for a smooth surface). "Seen" by the Brownian motion, the cubic Koch surface does not differ considerably with respect to a smooth surface. In particular, their physical transfer properties will not be too different. As a practical consequence, it would be difficult to distinguish the correlation exponent from 2 in a physical experiment.

ACKNOWLEDGMENTS

The authors thank Professor N.G. Makarov for critical remarks and valuable discussions of theoretical basis and numerical results, and Professor H. Hermann for helpful advice.

[1] P. Meakin, *Fractals, Scaling and Growth far from Equilibrium* (Cambridge University Press, Cambridge, England, 1998).
[2] J. B. Garnett and D. E. Marshall, *Harmonic Measure* (to be published).
[3] N. G. Makarov, Proc. London Math. Soc. **51**, 369 (1985).
[4] B. Sapoval, Phys. Rev. Lett. **73**, 3314 (1994).
[5] B. Sapoval, in *Fractals and Disordered Systems*, edited by A. Bunde and S. Havlin (Springer, New York, 1996), pp. 223–261.
[6] K. J. Falconer, *Fractal Geometry. Mathematical Foundations and Applications* (Wiley, Chichester, 1990).
[7] N. G. Makarov, St. Petersbg. Math. J. **10**, 217 (1999).
[8] P. Ossadnik, Physica A **176**, 454 (1991).
[9] T. C. Halsey and M. Leibig, Ann. Phys. **219**, 109 (1992).
[10] D. S. Grebenkov, Ph.D. thesis, Ecole Polytechnique (France) (2004).
[11] B. Sapoval, M. Filoche, K. Karamanos, and R. Brizzi, Eur. Phys. J. B **9**, 739 (1999).
[12] M. Filoche and B. Sapoval, Eur. Phys. J. B **9**, 755 (1999).
[13] P. Meakin, Phys. Rev. A **33**, 1365 (1986).
[14] M. Leibig and T. C. Halsey, J. Electroanal. Chem. **358**, 77 (1993).
[15] H. Ruiz-Estrada, R. Blender, and W. Dieterich, J. Phys.: Condens. Matter **6**, 10509 (1994).
[16] B. Duplantier, Phys. Rev. Lett. **82**, 880 (1999); **82**, 3940 (1999); **84**, 1363 (2000).
[17] B. Duplantier, J. Stat. Phys. **110**, 691 (2003).
[18] M. H. Jensen, A. Levermann, J. Mathiesen, and I. Procaccia, Phys. Rev. E **65**, 046109 (2002).
[19] M. H. Jensen, J. Mathiesen, and I. Procaccia, Phys. Rev. E **67**, 042402 (2003).
[20] C. J. G. Evertsz and B. Mandelbrot, J. Phys. A **25**, 1781 (1992).
[21] J. Bourgain, Invent. Math. **87**, 477 (1987).
[22] T. H. Wolff, in *Essays on Fourier Analysis in Honor of Elias M. Stein, Princeton Math. Ser., Vol. 42* (Princeton University Press, Princeton, N. J., 1995), pp. 321–384.